

Model Predictive Direct Current Control for Multi-Level Converters

Tobias Geyer, *Member, IEEE*

Abstract—A model predictive current controller for multi-level inverter driving electrical machines is proposed that keeps the stator currents within given bounds around their respective references and balances the inverter’s neutral point potential around zero. The inverter switch positions are directly set by the controller thus avoiding the use of a modulator. Admissible switching sequences are enumerated and a state-space model of the drive is used to predict the drive’s response to each sequence. The predicted short-term switching losses are evaluated and minimized. The concept of extrapolation and the use of bounds achieve an effective prediction horizon of up to 100 time-steps despite the short switching horizon. When compared to classic modulation schemes such as pulse width modulation, for long prediction horizons, the switching losses and/or the harmonic distortion of the current are almost halved when operating at low pulse numbers, thus effectively resembling the steady-state performance of optimized pulse patterns. During transients the dynamic response time of the proposed controller is in the range of a few ms and thus very fast.

Index Terms—Model predictive control, current control, medium-voltage drive

I. INTRODUCTION

In high power applications exceeding one megawatt multi-level inverters are typically used – rather than two-level inverters – in order to reduce the rating of the semiconductor switching devices, to minimize the harmonic distortions and to increase the modulated voltage. The inverter must be operated such that the desired three-phase load currents are produced. Several control methodologies are available to address this current control problem in three-phase voltage source inverters. As shown in the survey paper [1], the controllers can be grouped into linear and nonlinear control schemes.

The most prominent representative of a linear control methodology is Field Oriented Control (FOC), which is formulated in a rotating orthogonal reference frame [2]. Two (orthogonal) control loops are used, typically with Proportional Integral (PI) controllers augmented with feedforward terms – one for the torque producing and one for the flux producing current. A subsequent Pulse Width or Space Vector Modulator (PWM or SVM) translates the stator voltage reference signals into gating commands for the inverter [3]. Examples for non-linear current control schemes include hysteresis controllers, which typically directly set the inverter switch positions. In a drive setting the current control loop typically constitutes the inner loop within a cascaded control loop. On the machine side, the outer loop includes the torque and/or speed and the flux control loops, while on the grid side the active and reactive power is controlled.

T. Geyer is currently with the Department of Electrical and Computer Engineering, The University of Auckland, New Zealand; e-mail: t.geyer@ieec.org

Recently, the power electronics community has started to investigate the concept of Model Predictive Control (MPC) [4], [5]. The roots of MPC can be traced back to the process industry, where the origins of MPC were developed in the 1970s [6]. The emerging field of MPC for three-phase voltage source inverters can be divided into two categories. The first one builds on FOC and replaces the inner (current) control loop by MPC and keeps the modulator in place. Examples for this approach include [7] and [8]. In the second variety, MPC directly manipulates the inverter switch positions thus superseding a modulator. For Neutral Point Clamped (NPC) inverters the latter scheme is available with a prediction horizon of one as introduced in [9].

This paper proposes an MPC based model predictive current controller with very long prediction horizons in the range of 100 time-steps. Specifically, a Model Predictive Direct Current Controller (MPDCC) for multi-level inverter is proposed that keeps the stator currents within specified bounds around their references, balances the inverter’s neutral point potential(s) around zero and minimizes either the inverter switching losses or its switching frequency. The control problem is formulated in an orthogonal reference frame that can be either stationary or synchronously rotating. The formulation of the current bounds in different reference frames is compared with each other and with the bounds resulting from MPDTC. A modulator is not required, since the gating signals are directly synthesized by the controller.

The key benefit of this approach is that the current control and the modulation problems are addressed in one computational stage. As a result the current harmonic distortion and the switching losses can be reduced at the same time when compared to PWM. Indeed, at low switching frequencies, the resulting steady-state behavior is similar to the one obtained by Optimized Pulse Patterns (OPP). Yet, during transients, a very fast current response time is achieved in contrast to OPPs, which tend to be applicable only in very slow control loops.

This MPDCC scheme can be considered as an adaptation of Model Predictive Direct Torque Control (MPDTC) to the current control problem. This is achieved by changing the control objectives – namely, instead of controlling the torque and flux magnitude the stator currents are controlled. MPDTC was developed in early 2004, see [5] and [10], with prediction horizons in the range of a few dozen, experimentally verified on a 2.5 MVA drive in 2007 [11] and later generalized to enable even longer prediction horizons [12]. Preliminary results of a MPDCC scheme for a two-level inverter based on the initial MPDTC algorithm minimizing the inverter switching

frequency and using relatively short prediction horizons were presented in [13].

II. PHYSICAL MODEL OF THE DRIVE SYSTEM

Throughout this paper, we will use normalized quantities. Extending this to the time scale t , one time unit corresponds to $1/\omega_b$ seconds, where ω_b is the base angular velocity.

A. The $\alpha\beta 0$ Reference Frame

All variables $\xi_{abc} = [\xi_a \ \xi_b \ \xi_c]^T$ in the three-phase system (abc) are transformed to $\xi_{\alpha\beta 0} = [\xi_\alpha \ \xi_\beta \ \xi_0]^T$ in the orthogonal $\alpha\beta 0$ stationary reference frame through $\xi_{\alpha\beta 0} = P \xi_{abc}$. Using the $\alpha\beta 0$ reference frame and aligning the α -axis with the a -axis, the following transformation matrix is obtained

$$P = \frac{2}{3} \begin{bmatrix} 1 & -\frac{1}{2} & -\frac{1}{2} \\ 0 & \frac{\sqrt{3}}{2} & -\frac{\sqrt{3}}{2} \\ \frac{1}{2} & \frac{1}{2} & \frac{1}{2} \end{bmatrix}. \quad (1)$$

B. Physical Model of the Inverter

As an illustrative example for a variable speed drive system with a multi-level inverter consider a three-level Neutral Point Clamped (NPC) voltage source inverter driving an induction machine, as depicted in Fig. 1. The total dc-link voltage V_{dc} over the two dc-link capacitors x_c is assumed to be constant. Let the integer variables $u_a, u_b, u_c \in \{-1, 0, 1\}$ denote the switch positions in each phase leg – the so called phase states, where the values $-1, 0, 1$ correspond to the phase voltages $-\frac{V_{dc}}{2}, 0, \frac{V_{dc}}{2}$, respectively. Note that in a three-level inverter 27 different switch combinations exist. The actual voltage applied to the machine terminals is given by $v_{\alpha\beta 0} = 0.5V_{dc} P u_{abc}$ with $u_{abc} = [u_a \ u_b \ u_c]^T$.

The neutral point potential $v_n = 0.5(V_{dc,lo} - V_{dc,up})$ between the two capacitors floats. In here, $V_{dc,lo}$ and $V_{dc,up}$ denote the voltage over the lower and upper dc-link half, respectively. The neutral point potential changes when current is drawn directly from it, i.e. when one of the switch positions is zero. Taking into account that the phase currents sum up to zero, i.e. $i_{sa} + i_{sb} + i_{sc} = 0$, it is straightforward to derive

$$\frac{dv_n}{dt} = \frac{1}{2x_c} |u_{abc}|^T P^{-1} i_{s,\alpha\beta 0}, \quad (2)$$

where $i_{s,\alpha\beta 0}$ is the stator current expressed in the stator reference frame, and $|u_{abc}| = [|u_a| \ |u_b| \ |u_c|]^T$ is the componentwise absolute value of the inverter switch positions [5].

To avoid a shoot-through direct switching between the upper and lower rails is prohibited.

Switching losses arise in the inverter when turning the semiconductors on or off and commutating the phase current. These losses depend on the applied voltage, the commutated current and the semiconductor characteristics. Considering Integrated Gate Commutated Thyristors (IGCT), with the GCT being the semiconductor switch, the switch-on and switch-off losses can be well approximated to be linear in the dc-link voltage and the phase current. Yet for diodes, the reverse recovery losses are linear in the voltage, but nonlinear in the commutated current. As shown in [12], [14], the switching

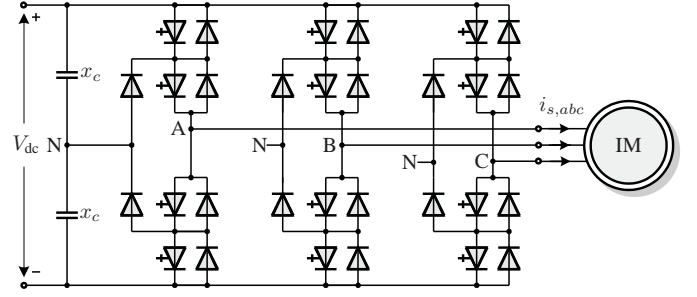


Fig. 1: Three-level neutral point clamped VSI driving an induction motor

losses can be derived as a function of the switching transition, the commutated phase current and its polarity.

C. Physical Model of the Machine

The state-space model of a squirrel-cage induction machine in the stationary $\alpha\beta$ reference frame is summarized hereafter. For the current control problem at hand it is convenient to choose the stator currents $i_{s\alpha}$ and $i_{s\beta}$ as state variables. The state vector is complemented by the rotor flux linkages $\psi_{r\alpha}$ and $\psi_{r\beta}$, and the rotor's angular velocity ω_r . The model input are the stator voltages v_α and v_β . The model parameters are the stator and rotor resistances r_s and r_r , the stator, rotor and mutual reactances x_{ls} , x_{lr} and x_m , respectively, the inertia J , and the mechanical load torque T_ℓ , where the rotor quantities are referred to the stator circuit.

The continuous-time state equations are [15], [16]

$$i_{s\alpha} + \tau_\sigma \frac{di_{s\alpha}}{d\tau} = \frac{k_r}{r_\sigma \tau_r} \psi_{r\alpha} + \frac{k_r}{r_\sigma} \omega_r \psi_{r\beta} + \frac{1}{r_\sigma} v_\alpha \quad (3a)$$

$$i_{s\beta} + \tau_\sigma \frac{di_{s\beta}}{d\tau} = \frac{k_r}{r_\sigma \tau_r} \psi_{r\beta} - \frac{k_r}{r_\sigma} \omega_r \psi_{r\alpha} + \frac{1}{r_\sigma} v_\beta \quad (3b)$$

$$\psi_{r\alpha} + \tau_r \frac{d\psi_{r\alpha}}{d\tau} = -\omega_r \tau_r \psi_{r\beta} + x_m i_{s\alpha} \quad (3c)$$

$$\psi_{r\beta} + \tau_r \frac{d\psi_{r\beta}}{d\tau} = \omega_r \tau_r \psi_{r\alpha} + x_m i_{s\beta} \quad (3d)$$

$$\tau_m \cdot \frac{d\omega_r}{d\tau} = T_e - T_\ell, \quad (3e)$$

with the electromagnetic torque

$$T_e = k_r (i_{s\beta} \psi_{r\alpha} - i_{s\alpha} \psi_{r\beta}). \quad (4)$$

The deduced parameters used in here are the coupling factor of the rotor $k_r = \frac{x_m}{x_r}$, the total leakage factor $\sigma = 1 - \frac{x_m^2}{x_s x_r}$, the equivalent resistance $r_\sigma = r_s + k_r^2 r_r$ and the leakage reactance $x_\sigma = \sigma x_s$, where $x_s = x_{ls} + x_m$ and $x_r = x_{lr} + x_m$. The deduced time constants include the transient stator time constant $\tau_\sigma' = \frac{\sigma x_s}{r_\sigma}$, the rotor time constant $\tau_r = \frac{x_r}{r_r}$ and the mechanical time constant $\tau_m = 1/J$.

III. CURRENT CONTROL PROBLEM

The control problem is to regulate the stator currents around their references. During transients a high dynamic performance is to be ensured, i.e. a short settling time in the range of a few ms. At steady state operating conditions the harmonic distortion of the current is to be minimized so as to reduce the copper losses and thus the thermal losses in the stator

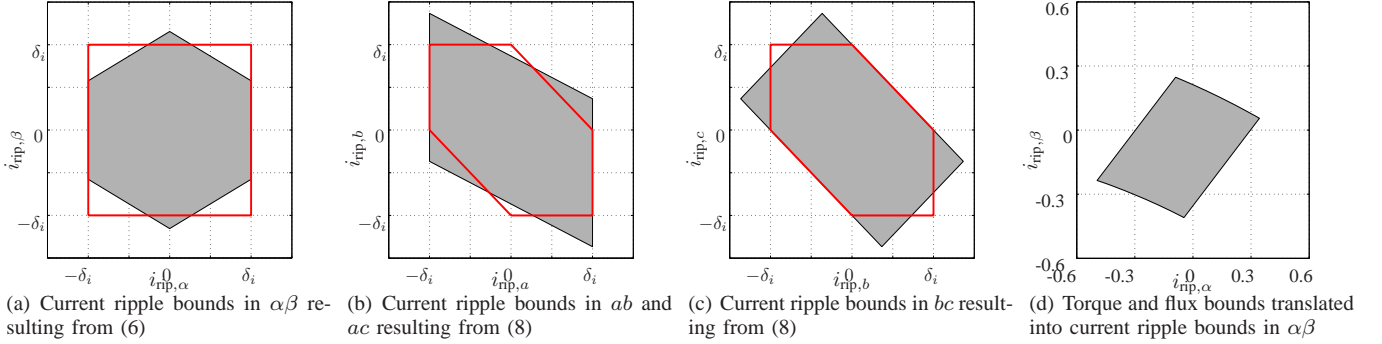


Fig. 2: Bounds on the current ripple in $\alpha\beta$, ab , ac and bc , when imposing current bounds in abc or in $\alpha\beta$, respectively. The right most figure shows the current ripple bounds in $\alpha\beta$ resulting from the torque and flux bounds imposed in model predictive direct torque control

winding of the machine. The current's harmonic distortion directly relates to the current ripple, which is defined as the deviation of the instantaneous current from its reference. Thus instead of reducing the current harmonic distortion we can also minimize the ripple current. The proportionality between the ripple and the harmonic distortion will be shown in Sect. VI-C.

With regards to the inverter the switching losses in the semiconductors are to be minimized. An indirect way of achieving this is to reduce the device switching frequency. The inverter's state(s) such as the neutral point potential has to be balanced around zero.

A suitable measure for the harmonic distortion of the current is the Total Demand Distortion (TDD)

$$I_{TDD} = \frac{\sqrt{0.5 \sum_{h \neq 0} I_h^2}}{I_{nom}}, \quad (5)$$

in which the nominal current I_{nom} refers to the operating condition at nominal speed and load of the drive. The (harmonic) Fourier components I_h , $h \geq 0$, can be differentiated into the fundamental current component I_0 and the h -th harmonic amplitude component I_h . The harmonic distortion of the electromagnetic torque is defined accordingly.

IV. FORMULATION OF THE STATOR CURRENT BOUNDS

The bounds on the stator currents can be imposed in various manners. Assume symmetric bounds around the current reference. Let δ_i denote the difference between the upper (lower) bound and the reference.

The natural choice [1] is to impose upper and lower bounds on the abc current of the form

$$|i_{rip,a}| \leq \delta_i, \quad |i_{rip,b}| \leq \delta_i, \quad |i_{rip,c}| \leq \delta_i, \quad (6)$$

where the ripple current in phase a is defined as $i_{rip,a} = i_{s,a} - i_{ref,a}$. The ripple currents in phase b and c are defined accordingly. Using (1) and taking into account that the ripple currents are common mode free (the machine's star point is not connected), the constraints (6) can be translated from the abc into the $\alpha\beta$ frame.

$$|i_{rip,\alpha}| \leq \delta_i, \quad |i_{rip,\alpha}| + \sqrt{3}|i_{rip,\beta}| \leq 2\delta_i \quad (7)$$

The set of ripple currents in $\alpha\beta$ that meet (6) is depicted in Fig. 2(a) as a gray polygon. The edges of the polygon are called facets. The facets are perpendicular to the a , b and c -axes, respectively. The distance of the facets to the origin is given by δ_i . The 0-component of the current ripple is always zero.

Conversely, one might impose upper and lower bounds on the currents in the $\alpha\beta$ frame as proposed e.g. in [13].

$$|i_{rip,\alpha}| \leq \delta_i, \quad |i_{rip,\beta}| \leq \delta_i \quad (8)$$

This constraint is visualized in Fig. 2(a) as a red square. Translating the set imposed by (8) from $\alpha\beta$ to abc yields a non-trivial shape. Fig. 2(b) shows the set in an orthogonal plane spanned by the a and b -axis, which is the same as for ac , while Fig. 2(c) shows the set in the bc plane. The red polygons in Figs. 2(b) and 2(c) refer to the constraint (6).

It is obvious that the two constraint formulations (6) and (8) lead to different sets in $\alpha\beta$ and abc . The current harmonic distortion relates to the ripple in abc rather than in $\alpha\beta$. Thus, from a TDD perspective, it is advantageous to impose the constraint (6) rather than (8). This is confirmed by simulation results, even though the difference amounts only to several percent and is thus fairly small. Since the machine model is formulated in $\alpha\beta$ it is convenient to formulate the current constraints also in this reference frame. Therefore, the constraint formulation (7), which is equivalent to (6), is adopted for MPDCC.

On the other hand, in a model predictive direct torque and flux control setting, i.e. MPDTC, the stator flux vector is the key figure to be controlled. Specifically, the angle between the stator and rotor flux vectors determines the electromagnetic torque, while the stator flux's magnitude is usually kept around its nominal value to keep the machine fully magnetized. By imposing upper and lower bounds on the torque and the stator flux magnitude a target window results that defines the ripple of the stator flux vector. Due to the direct correspondence between the stator flux and the stator current, the stator flux's target window can be translated into an equivalent window for the stator current ripple in $\alpha\beta$. The latter is shown in Fig. 2(d). Since the bounds on the stator flux magnitude are typically asymmetric, the set of ripple currents is also asymmetric with

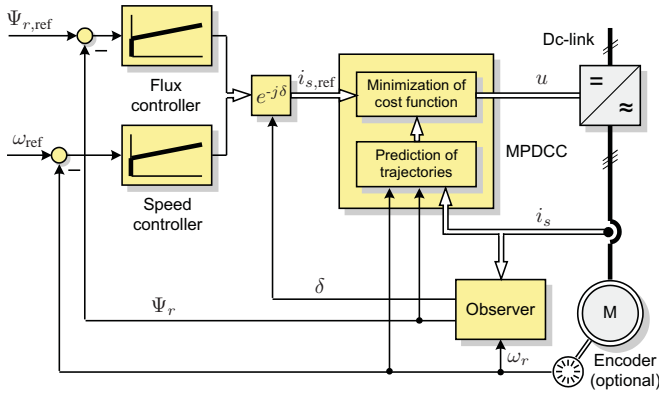


Fig. 3: Model predictive direct current control (MPDCC) for a multi-level voltage source inverter driving an electrical machine

respect to the origin. The curvature results from the bounds on the stator flux magnitude. Note that in $\alpha\beta$ this window rotates around the origin.

V. MODEL PREDICTIVE DIRECT CURRENT CONTROL

As shown in Fig. 3, MPDCC constitutes the inner current control loop formulated in the stationary $\alpha\beta$ reference frame. The current loop is augmented in a cascaded controller fashion by an outer loop that operates in the rotating dq frame and comprises a flux and a speed PI controller with feedforward terms.

A. Internal Controller Model

MPC relies on an internal model of the physical drive system to predict the future drive trajectories, specifically the current and neutral point trajectories.

The overall state vector of the drive is chosen to be $x = [i_{s\alpha} \ i_{s\beta} \ \psi_{r\alpha} \ \psi_{r\beta} \ v_n]^T$, the switch positions constitute the input vector $u = u_{abc} = [u_a \ u_b \ u_c]^T \in \{-1, 0, 1\}^3$, and the stator current along with the neutral point potential is the output vector $y = [i_{s\alpha} \ i_{s\beta} \ v_n]^T$. The rotor speed is assumed to be effectively constant within the prediction horizon, which turns the speed into a time-varying parameter. The prediction horizon being in the range of a few ms, this appears to be a mild assumption for medium-voltage drive applications. Nevertheless, including the speed as an additional state in the model might be necessary for highly dynamic drives and/or drives with a small inertia.

Combining the motor model (3)–(4) with the inverter model (2) and using the Euler formula, a discrete-time state-space model of the drive can be derived with the sampling interval $T_s = 25 \mu\text{s}$. The resulting state equation is bilinear in the input variable due to (2). The discrete-time model is omitted here due to space limitations, but it is conceptually similar to the one in [10].

B. Generalized MPDCC Algorithm

In MPDCC, the two stator current components are to be kept within given bounds around their respective references, while the neutral point potential is to be balanced around zero, see Fig. 3. For this, the inverter switch positions are directly set by

MPDCC thus making a modulator obsolete. A machine and an inverter model is used to assess possible switching sequences over a long prediction horizon. The switching sequence is chosen that minimizes the predicted inverter switching losses. Out of this sequence only the first gating signal (at the current time-instant) is applied.

Starting at the current time-step k , the MPDCC algorithm iteratively explores the tree of feasible switching sequences forward in time. At each intermediate step, all switching sequences must yield output trajectories that are either *feasible*, or *pointing in the proper direction*. We refer to these switching sequences as *candidate* sequences. Feasibility means that the output variable lies within its corresponding bounds; pointing in the proper direction refers to the case in which an output variable is not necessarily feasible, but the degree of the bound's violation decreases at every time-step within the switching horizon. The above conditions need to hold *componentwise*, i.e. for all three output variables¹.

It is important to distinguish between the switching horizon (number of switching instants within the horizon, i.e. the degrees of freedom) and the prediction horizon (number of time-steps MPC looks into the future). Between the switching instants the switch positions are frozen and the drive behavior is extrapolated until a hysteresis bound is hit. The concept of extrapolation gives rise to long prediction horizons (typically 30 to 100 time-steps), while the switching horizon is very short (usually one to three). The switching horizon is composed of the elements 'S' and 'E', which stand for 'switch' and 'extrapolate' (or more generally 'extend'), respectively. We use the task 'e' to add an optional extension leg to the switching horizon. For more details and visualizations about the concept of the switching horizon and its elements 'S', 'E' and 'e', the reader is referred to [12].

At time-step k , the generalized MPDCC algorithm computes the three-phase switch position $u(k)$ according to the following procedure.

- 1) Initialize the root node with the current state vector $x(k)$, the last switch position $u(k-1)$ and the switching horizon. Push the root node onto the stack.
- 2a) Take the top node with a non-empty switching horizon from the stack.
- 2b) Read out the first element. For 'S', branch on all feasible switch transitions. For 'E', extend the trajectories either by extrapolation as detailed in [5] or by using the internal controller model of Sect. V-A.
- 2c) Keep only the switching sequences that are candidates.
- 2d) Push these sequences onto the stack.
- 2e) Stop if there are no more nodes with non-empty switching horizons. The result of this are the predicted (candidate) switching sequences $U^i(k) = [u^i(k), \dots, u^i(k+n_i-1)]$ over the variable-length prediction horizons n_i , where $i \in \mathcal{I}$ and \mathcal{I} is an index set.

¹As an example, consider the case where the α -current component is feasible, the β -current component points in the proper direction and the neutral point potential is feasible.

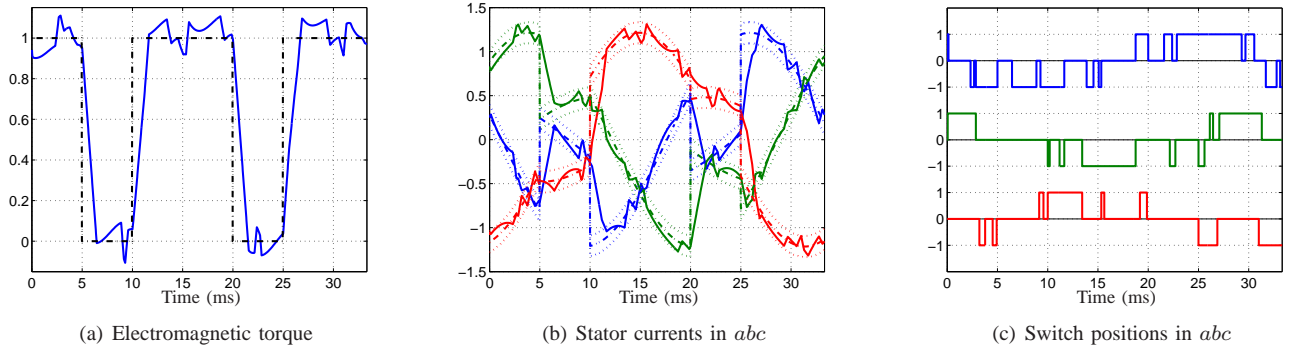


Fig. 4: Dynamic response of model predictive direct current control during torque steps of magnitude 1 pu. The torque reference with the torque response, the three-phase stator currents and the switch positions are shown versus the time-axis in ms. The rotor's angular velocity is $\omega_r = 0.6$ pu, the current bound width is $\delta_i = 0.12$ and the switching horizon is 'eSESE'

- 3) Compute for each (candidate) sequence $i \in \mathcal{I}$ the associated cost. If the switching frequency is to be minimized, consider $c_i = s_i/n_i$, which approximates the average switching frequency, where $s_i = \sum_{\ell=k}^{k+n_i-1} \|u_i(\ell) - u_i(\ell-1)\|_1$ is the total number of switch transitions in the switching sequence $U^i(k)$, and n_i is the corresponding sequence length. Conversely, if the losses are targeted, the cost function $c_i = E_i/n_i$ is used, where E_i denotes the switching losses.
- 4) Choose the switching sequence $U^* = U^i(k)$ with the minimal cost, where $i = \arg \min_{i \in \mathcal{I}} c_i$.
- 5) Apply (only) the first switch position $u(k) = u^*$ of this sequence and execute the above procedure at the next time-step $k+1$.

Alternatively, by adapting the drive model, MPDCC can also be formulated in a dq reference frame rotating synchronously with the rotor. In dq the current references are constant and so are the upper and lower bounds. Yet, the hexagon-shaped bounds, see Fig. 2(a), would rotate in the dq frame. A possible simplification would be to approximate the hexagon by a circle. Moreover, in dq , the voltage vectors depend on the angular position of the frame complicating the computation of the drive response in the MPDCC Step 2b).

The controller's computation time of one sampling interval has been neglected above. Using the internal controller model of the drive and the previously chosen switch position, this delay can be easily compensated by translating the measurements one time-step forward. For more details, see [11].

VI. PERFORMANCE EVALUATION

As a case study, consider a three-level NPC voltage source inverter driving an induction machine as shown in Fig. 1. A 3.3 kV and 50 Hz squirrel-cage induction machine rated at 2 MVA is used as an example for a commonly used medium-voltage induction machine. The machine and inverter parameters are summarized in Table I. The semiconductors used are ABB's 35L4510 4.5 kV 4 kA IGCT and ABB's 10H4520 fast recovery diode. The pu system is established using the base quantities $V_B = \sqrt{2/3}V_{\text{rat}} = 2694$ V, $I_B = \sqrt{2}I_{\text{rat}} = 503.5$ A and $f_B = f_{\text{rat}} = 50$ Hz. As previously, δ_i denotes the width

of the bounds on the abc current components, which are symmetric around the reference, where δ_i is equal to the upper bound minus the reference.

A. Transients

At 60% speed steps of magnitude 1 pu in the torque reference are applied to MPDCC. As shown in Fig. 4 a very fast current and thus torque response is achieved limiting the length of the transients to about 1.5 ms. It is apparent from the control algorithm described in Sect. V that MPDCC is similarly fast as deadbeat and hysteresis control schemes. Note that excessive switching during the transients is avoided as can be seen from Fig. 4(c).

B. Steady-State Operation

At 60% speed and full torque closed-loop simulations were run to evaluate MPDCC's performance at steady-state conditions. The key performance criteria here are the harmonic distortions of the current and the torque, and the switching losses in the inverter. This performance evaluation is done for switching horizons of varying length and various bounds. MPDCC is compared with two well-established modulation methods: PWM/SVM and optimized pulse patterns (OPP).

Specifically, a three-level regular sampled PWM is used with two triangular carriers, which are in phase (phase disposition). It is generally accepted that for multi-level inverters carrier-based PWM with phase disposition (PD) results in the lowest harmonic distortion. As shown in [17] – by adding a

Induction Motor			
Voltage	3300 V	r_s	0.0108 pu
Current	356 A	r_r	0.0091 pu
Real power	1.587 MW	x_{ls}	0.1493 pu
Apparent power	2.035 MVA	x_{lr}	0.1104 pu
Frequency	50 Hz	x_m	2.3489 pu
Rotational speed	596 rpm		
Inverter			
Dc-link voltage	5200 V	V_{dc}	1.930 pu
		x_c	11.769 pu

TABLE I: Rated values (left) and parameters (right) of the drive

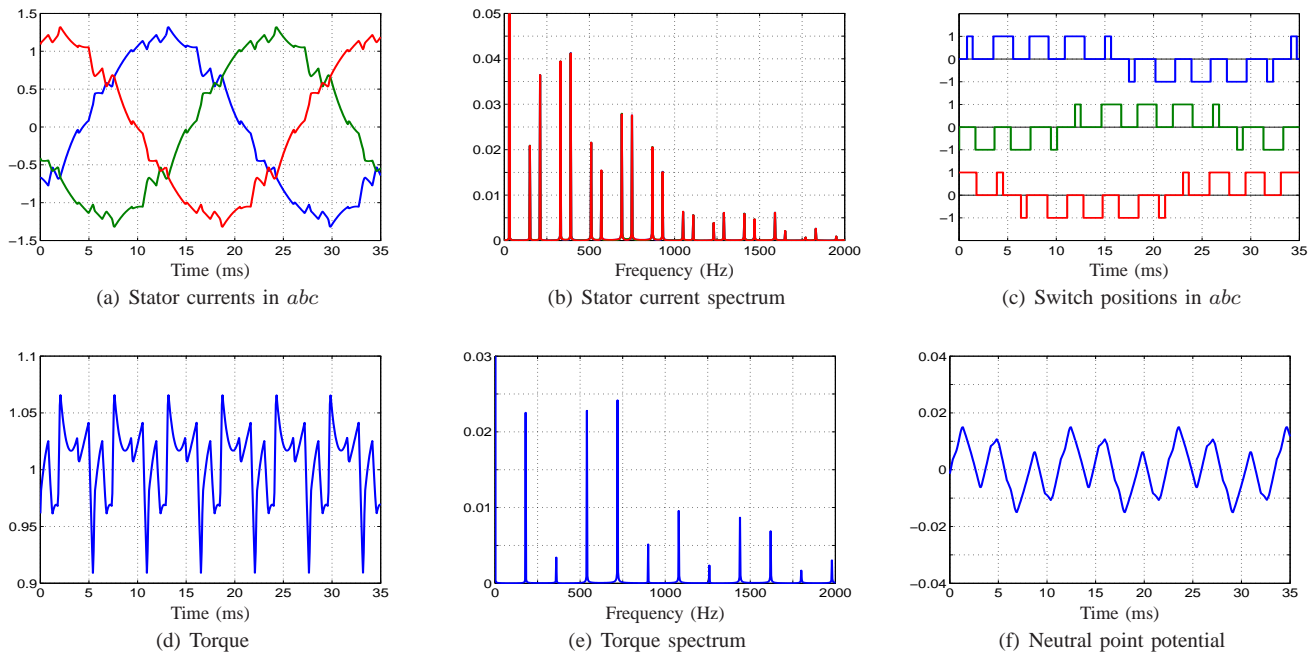


Fig. 5: Field oriented control with PWM/SVM and the carrier frequency $f_c = 270$ Hz at 60% speed and full torque. The stator currents and the torque in the time- and frequency-domain, as well as the the neutral point potential and the switch positions with the stator currents are shown versus the time-axis in ms. All quantities are given in pu

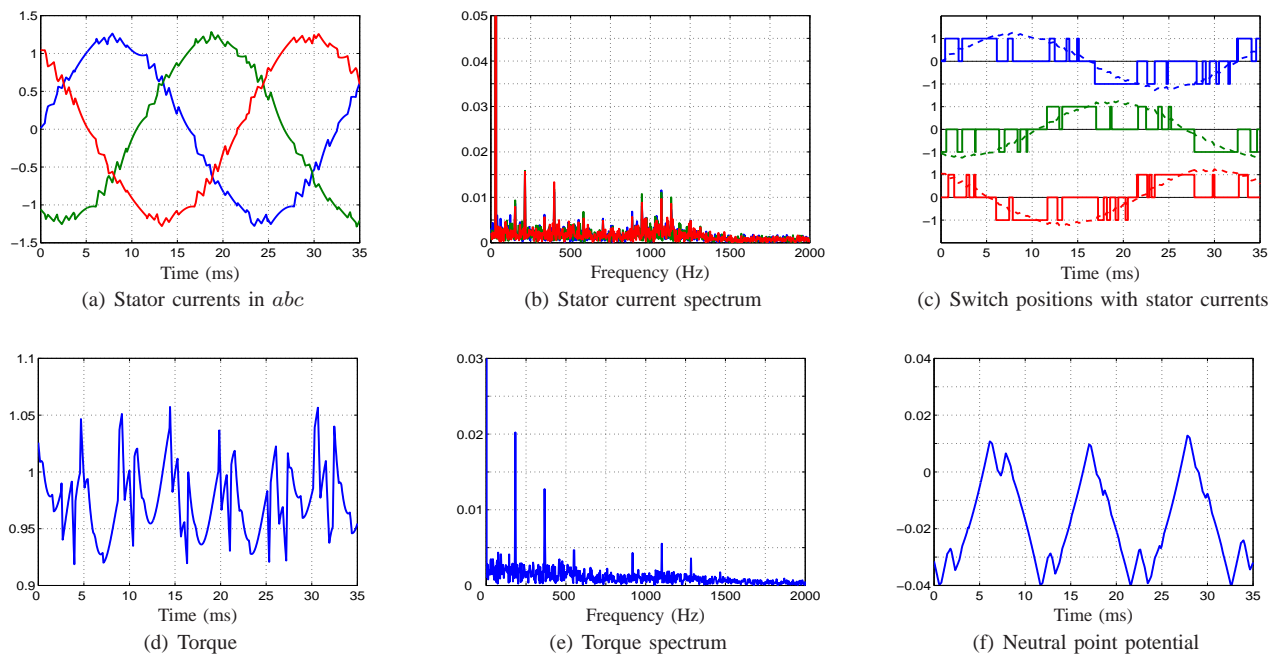


Fig. 6: Model predictive direct current control with the current bound $\delta_i = 0.0825$. The switching horizon 'eSESESE' leads here to a prediction horizon of 70 time-steps on average. The operating point, the plots and their scaling are the same as in Fig. 5 to facilitate a direct comparison

proper common mode voltage to the reference voltage, which is of the min/max type plus a modulus operation – PWM with PD is equivalent to SVM, in the sense that both methods yield the same gating signals.

Alternatively, optimized pulse patterns can be calculated in an off-line procedure by computing the optimal switching angles over one fundamental period for all possible operating

points [18] by minimizing the current distortion for a given switching frequency (pulse number). OPPs are typically used in a very slow control loop like V/f control, which is also employed here for the OPPs.

As shown in Fig. 5, PWM/SVM with the carrier frequency $f_c = 270$ Hz leads to distinctive current and torque spectra around multiples of f_c . The switching pattern is fairly uni-

Control scheme	Control setting	Switching horizon	Avg. pred. horizon	P_{sw} [kW]	f_{sw} [Hz]	$I_{s,TDD}$ [%]	$T_{e,TDD}$ [%]	P_{sw} [%]	f_{sw} [%]	$I_{s,TDD}$ [%]	$T_{e,TDD}$ [%]
PWM/SVM	$f_c = 90$ Hz	–	–	2.44	60.0	14.6	4.37	100	100	100	100
MPDCC	$\delta_i = 0.195$	eSE	54.9	1.12	61.0	9.02	4.76	45.9	102	61.7	109
MPDCC	$\delta_i = 0.1925$	eSESE	112	1.12	61.0	8.97	4.80	45.9	102	61.3	110
MPDCC	$\delta_i = 0.18$	eSESESE	177	1.15	61.0	8.60	4.44	47.1	102	58.0	102
OPP	$d = 2$	–	–	1.92	60.0	8.18	3.76	78.7	100	55.9	86.0
PWM/SVM	$f_c = 270$ Hz	–	–	4.15	150	7.69	3.11	100	100	100	100
MPDCC	$\delta_i = 0.115$	eSE	20.9	4.00	195	7.32	5.91	96.4	130	95.2	190
MPDCC	$\delta_i = 0.1$	eSESE	54.6	3.94	169	5.55	3.77	94.9	113	72.2	121
MPDCC	$\delta_i = 0.0825$	eSESESE	70.5	4.02	199	4.56	2.96	96.9	133	59.3	95.2
OPP	$d = 5$	–	–	4.18	153	4.31	2.24	101	102	56.0	72.0
PWM/SVM	$f_c = 720$ Hz	–	–	9.90	375	2.83	1.19	100	100	100	100
MPDCC	$\delta_i = 0.046$	eSE	10.4	9.83	423	2.74	2.12	99.3	113	96.8	178
MPDCC	$\delta_i = 0.0450$	eSESE	21.1	9.81	451	2.21	1.52	99.1	120	78.1	128
MPDCC	$\delta_i = 0.039$	eSESESE	29.9	9.77	494	2.20	1.38	98.7	132	77.7	116
OPP	$d = 13$	–	–	10.4	396	2.16	0.99	105	106	76.3	83.2

TABLE II: Comparison of MPDCC with PWM/SVM and OPP in terms of switching losses P_{sw} , switching frequency f_{sw} , current TDD $I_{s,TDD}$ and torque TDD $T_{e,TDD}$. The center part shows absolute values, while the values in the right part are relative using PWM as a baseline. The three sets of comparisons refer to a switching frequency of about 60 Hz, and switching losses of around 4 and 10 kW. The operating point is at 60% speed and nominal torque

formly distributed over a fundamental period. The resulting switching losses are 4.15 kW and the current TDD is 7.7% as summarized in Table II. The MPDCC bounds are tuned such that similar switching losses are obtained. As the switching horizon is increased the average prediction horizon increases, too, allowing MPDCC to make better informed decision by looking further into the future. As a result, the bounds can be tightened and thus the harmonic distortions of the current and the torque are reduced while keeping the switching losses constant. This can be seen in Fig. 6, which shows the results for MPDCC with a long switching horizon and fairly tight bounds. For the same switching losses, the current distortion is reduced by 40% while the torque distortion is also marginally improved. The switching frequency, however, tends to be higher than in PWM since it is not directly minimized. By arranging the switching pattern such that a significant proportion of the switching transitions occurs when the phase currents and thus the losses are small, the switching losses are kept at the same level as with PWM/SVM despite the higher switching frequency. Interestingly enough, in terms of switching losses and current distortions, MPDCC with long horizons effectively resembles the performance of OPPs – refer to the OPP with pulse number $d = 5$. The torque distortions, however, are worse.

Alternatively, one may wish to minimize the switching losses with regards to PWM/SVM while keeping the current TDD constant. As an example consider again PWM with $f_c = 270$ Hz. MPDCC with the long switching horizon ‘eSESESE’, prediction horizon of 177 steps and bound width $\delta_i = 0.18$ leads to 12% higher current distortions, but the switching losses are reduced from 4.15 down to 1.15 kW, i.e. by 71%! In this case, MPDCC actually outperforms the OPP with pulse number $d = 2$ (40% less switching losses while the current and torque distortions are not dissimilar). This might appear to be counter-intuitive, since it is often assumed that OPPs provide the upper bound on the achievable steady-state

performance of a modulator. Yet, the OPPs were computed by minimizing only the current distortions, not considering the switching losses. By also taking the switching losses into account and by accordingly rearranging the pulses as shown in Fig. 7, MPDCC is able to achieve similarly low distortions, while further reducing the switching losses, see Table III. Yet, MPDCC is particularly effective to yield low current distortions, but less effective to reduce the torque distortion, as motivated in Sect. IV.

The benefit of MPDCC is particularly pronounced when operating at small pulse numbers. For a switching frequency of about 60 Hz MPDCC reduces both the switching losses and the current TDD by about 50% when compared to PWM with the carrier frequency of 90 Hz. For higher switching frequencies, however, the gain is less significant, as demonstrated by the benchmarking with respect to PWM with $f_c = 720$ Hz. This characteristic can be also observed with OPPs, whose performance benefit drops as the pulse number is increased, see Table II.

C. Tuning

In MPDCC the width of the current bounds is a tuning parameter that sets the trade-off between the level of harmonic distortion and the switching losses. This tuning parameter is equivalent to the carrier frequency in PWM/SVM. Specifically, by tightening the current bounds, the current ripple is reduced

	OPP				MPDCC			
i_a [pu]	-0.74	0.66	1.16	1.09	0.20	1.32	0.42	0.62
E_{on} [J]	0.19				0.03	0.07		
E_{off} [J]	1.57	1.41	2.32		2.81		1.33	
E_{rr} [J]	2.07		3.24		0.57	1.18		
$\sum E$ [J]	10.8				6.00			

TABLE III: Switching losses E for the positive halfwaves in phase a shown in Fig. 7. E_{on} , E_{off} and E_{rr} denote the GCT turn-on, GCT turn-off and the diode reverse recovery losses, respectively. MPDCC’s switching losses are here 45% less than the ones of the OPP, which is in line with Table II

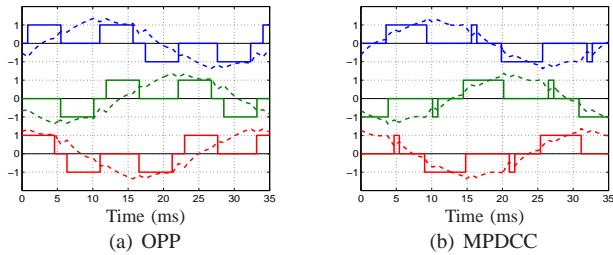


Fig. 7: Comparison of the abc switching patterns of an OPP with $d = 2$ and MPDCC with the switching horizon 'eSESE' and the bound width $\delta_i = 0.18$. Both schemes yield the same switching frequency of about 60 Hz

and so are the current and torque TDDs. Over a wide range of the relation between the current ripple and the harmonic distortion appears to be linear, as can be seen from Fig. 8.

VII. CONCLUSIONS AND DISCUSSION

The operation of medium-voltage drives is usually confined to low switching frequencies in the range of a few 100 Hz. Under these conditions MPDCC can achieve switching losses and current distortion levels that are comparable to the ones typically achieved with OPPs. For very low pulse numbers MPDCC might even outperform OPPs in this respect. To minimize the torque distortion, however, MPDTC appears to be better suited, see also [19]. The shape of the current ripple sets is responsible for this difference.

Long horizons drastically improve the performance. Long horizons are achieved by combining the concept of extrapolation with the notion of imposing bounds on the controlled variables. Yet, when compared to FOC or DTC, the computational burden tends to be high. For short switching horizons a successful implementation was shown in [11]. To implement long switching horizons techniques from mathematical programming such as branch and bound can be used as explained in [20].

In this paper a three-level NPC inverter was used as a commonly used and illustrative example for a multi-level voltage source inverter. It is a matter of changing the internal controller model and thus a straightforward undertaking to address other topologies and machines.

ACKNOWLEDGMENT

The author would like to thank Georgios Papafotiou and Frederick Kieferndorf of ABB Corporate Research, Baden-Dättwil, Switzerland for the optimized pulse patterns used as a benchmark and support with the SVM modulator, respectively.

REFERENCES

- [1] M. P. Kazmierkowski and L. Malesani. Current control techniques for three-phase voltage-source pwm converters: A survey. *IEEE Trans. Ind. Electron.*, 45(5):691–703, Oct. 1998.
- [2] F. Blaschke. A new method for the structural decoupling of ac induction machines. In *IFAC Symposium*, pages 1–15, Oct. 1971.
- [3] J. Holtz. Pulsewidth modulation – a survey. *IEEE Trans. Ind. Electron.*, 32(5):410–420, Dec. 1992.
- [4] R. Kennel, A. Linder, and M. Linke. Generalized predictive control (GPC) – ready for use in drive applications? In *Proc. IEEE Power Electron. Spec. Conf.*, pages 1839–1844, Vancouver, Canada, 2001.

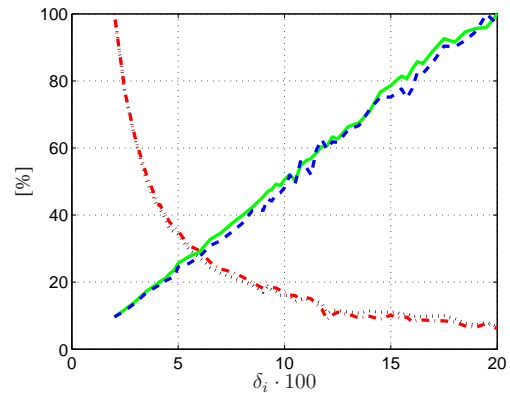


Fig. 8: Tuning of MPDCC: Current TDD (straight green line), the torque TDD (dashed blue line), the switching losses (dash-dotted red line) and the device switching frequency (dotted black line) vs the width of the current bound δ_i for MPDCC with the switching horizon 'eSE' at 60% speed and full torque. All four curves are given in percent and normalized to their maximum value in the interval $\delta_i = [0.02, \dots, 0.2]$

- [5] T. Geyer. *Low Complexity Model Predictive Control in Power Electronics and Power Systems*. PhD thesis, Automatic Control Laboratory ETH Zurich, 2005.
- [6] D. Q. Mayne, J. B. Rawlings, C. V. Rao, and P. O. M. Scokaert. Constrained model predictive control: Stability and optimality. *Automatica*, 36(6):789–814, Jun. 2000.
- [7] A. Linder and R. Kennel. Model predictive control for electrical drives. In *Proc. IEEE Power Electron. Spec. Conf.*, pages 1793–1799, Recife, Brasil, 2005.
- [8] S. Mariethoz, A. Domahidi, and M. Morari. Sensorless explicit model predictive control of permanent synchronous motors. In *Proc. IEEE Int. Electr. Mach. and Drive Conf.*, pages 1492–1499, Miami, Florida, USA, May 2009.
- [9] R. Vargas, P. Cortés, U. Ammann, J. Rodríguez, and J. Pontt. Predictive control of a three-phase neutral-point-clamped inverter. *IEEE Trans. Ind. Electron.*, 54(5):2697–2705, Oct. 2007.
- [10] T. Geyer, G. Papafotiou, and M. Morari. Model predictive direct torque control - part I: Concept, algorithm and analysis. *IEEE Trans. Ind. Electron.*, 56(6):1894–1905, Jun. 2009.
- [11] G. Papafotiou, J. Kley, K. G. Papadopoulos, P. Bohren, and M. Morari. Model predictive direct torque control - part II: Implementation and experimental evaluation. *IEEE Trans. Ind. Electron.*, 56(6):1906–1915, Jun. 2009.
- [12] T. Geyer. Generalized model predictive direct torque control: Long prediction horizons and minimization of switching losses. In *Proc. IEEE Conf. on Decis. and Control*, Shanghai, China, Dec. 2009.
- [13] J. C. Ramirez Martinez, R. M. Kennel, and T. Geyer. Model predictive direct current control. In *Proc. IEEE Int. Conf. on Ind. Techn.*, Viña del Mar, Chile, Mar. 2010.
- [14] S. Mastellone, G. Papafotiou, and E. Liakos. Model predictive direct torque control for MV drives with LC filters. In *Proc. Eur. Power Electron. Conf.*, Barcelona, Spain, Sep. 2009.
- [15] J. Holtz. The representation of AC machine dynamics by complex signal graphs. *IEEE Trans. Ind. Electron.*, 42(3):263–271, jun 1995.
- [16] P. C. Krause, O. Wasynczuk, and S. D. Sudhoff. *Analysis of Electric Machinery and Drive Systems*. Intersci. Publ. John Wiley & Sons Inc., 2nd edition, 2002.
- [17] B. P. McGrath, D. G. Holmes, and T. Lipo. Optimized space vector switching sequences for multilevel inverters. *IEEE Trans. Power Electron.*, 18(6):1293–1301, Nov. 2003.
- [18] G. S. Buja. Optimum output waveforms in PWM inverters. *IEEE Trans. Ind. Appl.*, 16(6):830–836, Nov./Dec. 1988.
- [19] T. Geyer. A comparison of control and modulation schemes for medium-voltage drives: emerging predictive control concepts versus field oriented control. In *Proc. IEEE Energy Conv. Congr. and Exp.*, Atlanta, USA, Sep. 2010.
- [20] T. Geyer. Computationally efficient model predictive direct torque control. In *Proc. IEEE Energy Conv. Congr. and Exp.*, Atlanta, USA, Sep. 2010.